



A comparison of adsorbate-induced faceting on flat and curved crystal surfaces

Andrzej Szczepkowicz ^{a,*}, Antoni Ciszewski ^a, Robert Bryl ^a, Czesław Oleksy ^b,
Cheng-Hsun Nien ^{c,1}, Qifei Wu ^{c,2}, Theodore E. Madey ^c

^a *Institute of Experimental Physics, University of Wrocław, Plac Maksa Borna 9, 50-204 Wrocław, Poland*

^b *Institute of Theoretical Physics, University of Wrocław, Plac Maksa Borna 9, 50-204 Wrocław, Poland*

^c *Department of Physics and Astronomy and Laboratory for Surface Modification, Rutgers—The State University of New Jersey, 136 Frelinghuysen Road, Piscataway, NJ 08854-8019, USA*

Received 4 July 2005; accepted for publication 16 September 2005

Available online 27 October 2005

Abstract

Adsorbate-induced thermal faceting on flat and curved crystal surfaces is compared. Two adsorption systems are investigated: O/W and Pd/W. Each of these systems is studied by two experimental techniques: scanning tunneling microscopy (flat surface), and field ion microscopy (curved surface). The experimental results are in accord with a solid-on-solid model applied for planar and spherical crystal shapes. Both experimental and theoretical results show that the shape of the facets is different for flat and curved surfaces, but the distance between the parallel facet edges is comparable.

© 2005 Elsevier B.V. All rights reserved.

Keywords: Faceting; Surface topography; Tungsten; Palladium; Oxygen; Scanning tunneling microscopy; Field ion microscopy; Monte Carlo simulations

1. Introduction

The aim of this paper is to compare adsorbate-induced faceting on flat and curved metal surface. Although adsorbate-induced faceting of metals has been studied both on flat (see for example [1–13]) and curved surfaces (e.g. [14–24]), so far there were only a few attempts [18–21] to correlate these experiments, that is, to study the same

* Corresponding author. Fax: +48 71 3287365.

E-mail address: asz2004@ifd.uni.wroc.pl (A. Szczepkowicz).

¹ Present address: Department of Physics, National Central University, Jhongli City, Taoyuan County 32001, Taiwan.

² Present address: Chemistry Department, Brookhaven National Laboratory, Upton, NY 11973.

physical process (the same adsorption system, similar coverages, length scales, temperatures) in the two geometries (different initial conditions). In this paper, we discuss the experimental and mathematical simulation results; we analyse the shape of the facets and obtain quantitative information about the facet dimensions, and the correlation of the facet sizes on flat and curved surfaces.

The dependence of the faceted topography on the initial crystal shape is a manifestation of the fact that equilibrium is not achieved in most faceting experiments, due to kinetic limitations. A hill-and-valley topography is usually observed, and the facets do not exceed a certain size ($\ll 1 \mu\text{m}$). Only under special conditions (small crystal, high annealing temperature, high desorption temperature of the adsorbate), is it possible to approach equilibrium and observe global, convex faceting, with no valleys [22,25].

An interesting general observation is that planar surfaces of many metals undergo facet formation when they are covered with oxygen or other adsorbates, and are annealed to elevated temperature. These include bcc W(111) and Mo(111), fcc Ir(210), Pt(210), Ni(210), and various Cu surfaces [7–13,26,27]. All of these are atomically-rough, non-close-packed surfaces with relatively high surface free energies. The presence of adsorbate increases the anisotropy in surface free energy, as well as lowering the average surface free energy. The increased anisotropy means that the faceted surface with its higher exposed surface area has a lower energy than the initially planar surface. Thus, faceting is driven by thermodynamics—the minimization of total surface free energy—but is controlled by the kinetics of diffusion, nucleation and growth.

In this paper, we have gathered data on the faceting behavior of two adsorption systems: Pd/W (Section 3) and O/W (Section 4), on two types of substrate samples: planar W(111) crystals and needle-shaped W crystals with curved apex surfaces. These are probably the only examples of faceting that have been studied in both geometries by microscopic techniques capable of imaging nanometer-scale facets.

In Section 5 we apply a solid-on-solid model to compare the faceting of flat and spherical surfaces.

The model used for simulations includes temperature as one of the parameters, allowing us to study the changes of the faceted topography with annealing temperature.

Our primary goal in this paper, not attempted in previous publications, is to compare quantitatively the dimensions of the facets on flat and curved surfaces. We carry out this comparison using both experimental and simulation results as discussed in Section 6. In particular, we investigate how the the distance between the parallel facet edges observed on spherical surfaces is related to the base length of pyramids observed on planar crystals. Also, for the first time we measure surface rms roughness of the faceted planar crystals, and describe quantitatively the correlation of this parameter with the facet size.

2. Quantitative analysis of the facet sizes

The experimental procedures used for FIM and STM measurements have been described in detail previously [20,22,28,29], and are summarized briefly in Sections 3 and 4 below.

In the experiments described in this work, we focus on the $\{211\}$ facets ((211), (121), and (112)) on the faceted surface (on a spherical crystal other facets can also be found, but we restrict our study to the vicinity of the (111) crystal pole; on the planar Pd/W(111) surface, $\{110\}$ facets can be found under certain conditions [30]). On an initially flat W(111) surface, adsorbate-induced pyramid-like $\{211\}$ facets are formed. On an initially curved W surface, steplike $\{211\}$ facets are formed. The faceting transition for the two cases is schematically depicted in Fig. 1. The facets are interconnected by edges oriented along $\langle 311 \rangle$ directions ($[3\bar{1}\bar{1}]$, $[\bar{1}3\bar{1}]$, and $[\bar{1}\bar{1}3]$).

In both geometries, the size of the facets can be characterized by the distance d_e between adjacent convex facet edges (Fig. 1). For the initially flat crystal, a more convenient parameter is the linear-base-size of the pyramid, where the base plane is chosen at the level of the average height. The intersection of a $\{211\}$ facet with the base plane is a segment; the length of this segment is the

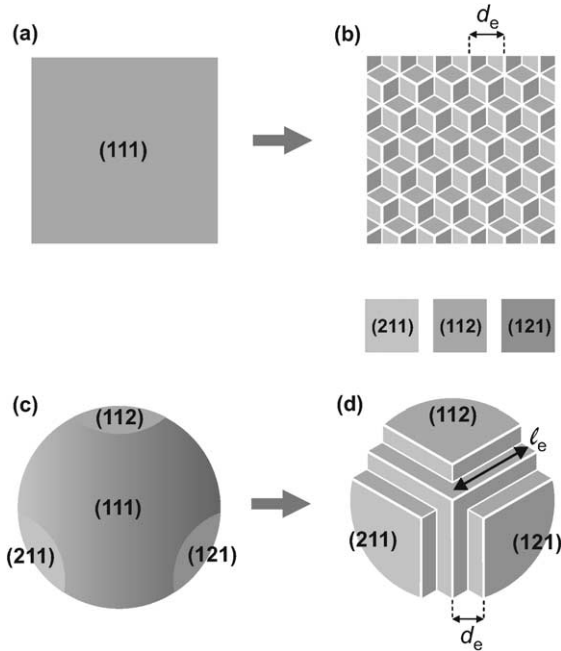


Fig. 1. The formation of $\{211\}$ facets on a flat crystal: (a), (b), and on a spherical crystal: (c), (d).

linear-base-size d_b , as shown in Fig. 2. For the idealized case, with all of the facets of the same size, the two parameters are equal: $d_e = d_b$.

The shape of the $\{211\}$ facets is different for flat and curved surfaces. For the initially flat surface, each facet is a rhombus with the area of $A(\text{flat}) = \frac{\sqrt{6}}{8} d_b^2 = 0.306 d_b^2$. For the initially curved surface, a typical facet is an elongated strip of width $\frac{\sqrt{33}}{11} d_e = 0.522 d_e$. The area of a facet is $A(\text{curved}) = 0.522 d_e \ell_e$, where ℓ_e denotes the length of the strip (edge length, Fig. 1d).

In contrast to the simplified situation depicted in Figs. 1 and 2, where all of the $\{211\}$ facets are of the same size, on a real faceted surface there is a coexistence of $\{211\}$ facets of various sizes. The actual distribution of the pyramid base sizes can be represented by a histogram. More briefly, the size distribution can be characterized by two parameters: (1) the *expected size* of the pyramids, (2) the *spread* of pyramid sizes. There are two natural candidates for the first parameter. If we identify and number all of the pyramids in the field of view, then pick a random number i and ask *What is the expected size*

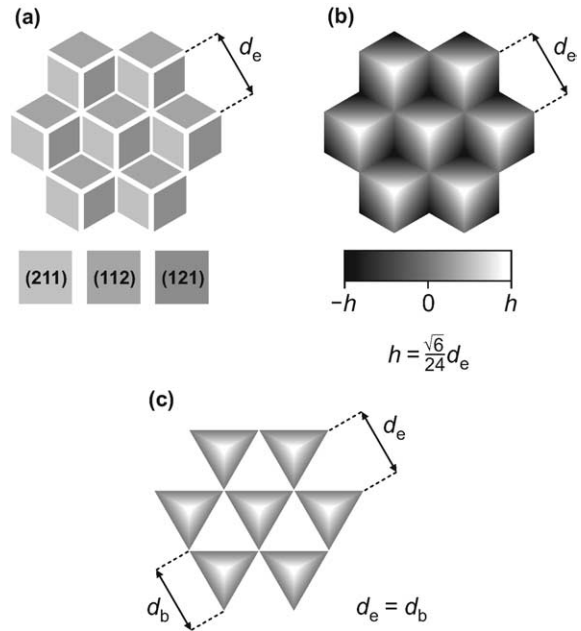


Fig. 2. Different graphical representations of $\{211\}$ facets formed on an initially flat (111) surface. (a) “Slope-filtered view”, where each surface orientation has a constant brightness level assigned to it. (b) “Height view”, with brightness corresponding to the height above the average level. (c) “Pyramid view”, where only the material above the average plane is shown.

of the pyramid number i ? then the answer is the arithmetic mean $\langle d_b \rangle = (\sum_{i=1}^n (d_b)_i) / n$. However, if we pick at random a point on the surface and ask *What is the expected size of the pyramid at this point?*, then the answer is quite different: the *weighted mean* $(\sum_{i=1}^n w_i \times (d_b)_i) / (\sum_{i=1}^n w_i)$, where the weights are proportional to the area occupied by the pyramids: $w_i = (d_b)_i^2$. In this paper, we choose the first possibility, following previous work [31]. For the second parameter, the *spread*, we choose the standard deviation:

$$\sigma(d_b) = \sqrt{\frac{1}{n} \sum_{i=1}^n ((d_b)_i - \langle d_b \rangle)^2}$$

The degree of topographic rearrangement occurring during faceting can be characterized by surface rms roughness (root mean square height deviation from the original flat surface): $\text{rms}(z) = \sigma(z) = \sqrt{\frac{1}{XY} \int (z(x,y) - \langle z \rangle)^2 dx dy}$, where X, Y are the width and length of the scanning region, and

$(z(x, y) - \langle z \rangle)$ is the height at point (x, y) , relative to the average plane. For practical purposes, $\text{rms}(z)$ can be expressed as $\sqrt{\frac{1}{P} \sum_{p=1}^P (z_p - \langle z \rangle)^2}$, where P is the number of pixels (data points) in the scanning region, and $(z_p - \langle z \rangle)$ is the height of the surface at point p , relative to the average plane.

For the ideal flat surface (Fig. 1(a)), $\text{rms}(z) = 0$. For the ideal faceted surface (Fig. 1(b)), integration yields $\text{rms}(z) = \frac{1}{24} d_b$.

3. Palladium on tungsten

Faceting of tungsten induced by a palladium overlayer has been studied by a variety of surface science techniques: low energy electron diffraction (LEED), Auger electron spectroscopy (AES), thermal desorption spectroscopy (TDS) [32], scanning tunneling microscopy (STM) [28,30,33], low energy ion scattering (LEIS) [31,34], soft X-ray photoelectron spectroscopy (SXPS) [7,30,35], field emission microscopy (FEM) [18,36] and field ion microscopy (FIM) [20,37].

It has been established that planar W(111) covered with one physical monolayer (PML) of Pd is unstable upon heating: massive faceting reconstruction occurs when the surface is heated above 700 K. As a result the surface is covered with pyramidal facets exposing {211}-type planes [32], as shown schematically in Fig. 2. (Note that one physical monolayer has the areal density of all exposed atomic layers; for W(111), this is 1.7×10^{15} atoms/cm². In contrast, one geometrical monolayer is the areal density of the topmost atomic layer, 5.8×10^{14} atoms/cm².)

The pyramid base lengths are 3–15 nm; the facet sizes increase with annealing temperature [7,28,31]. Prolonged annealing may lead to the formation of small (<3 nm) {110} pyramids [30]. The edges of the {211} pyramidal facets are slightly truncated; they have {332} orientations and are aligned along $\langle 311 \rangle$ directions [20,28].

Palladium forms a pseudomorphic Pd overlayer on a tungsten bcc bulk structure [28]. A single PML of palladium remains on the surface upon annealing (“floats”), [7,34]. Palladium in excess

of 1 PML is found to agglomerate into clusters [20,28,30]. Depending on the annealing time and temperature, the dominant features formed by this extra palladium can range from disordered patches, to large crystalline clusters sitting on the fully faceted surface [28]. Some tungsten is dissolved within these clusters [9,35].

On a curved tungsten surface, Pd-induced {211} and {110} facets have been observed after annealing at 900–1200 K [18,20,36]. In the vicinity of the (111) pole only the {211} facets have been detected [20].

3.1. Flat surface: Microscopic data (STM)

For observations of Pd/W faceting, the crystal surface is first cleaned [28], then covered with ~ 1.5 PML of palladium at ~ 300 K. This is followed by annealing for 3–7 min at the desired annealing temperature T_a . After the crystal has cooled down to room temperature (full thermal equilibration with the STM instrument took up to 5 h), STM analysis was carried out.

The STM images reveal {211} hill-and-valley faceting, consistent with the scheme shown in Fig. 2. A typical STM image obtained after 1075 K annealing is shown in Fig. 3.

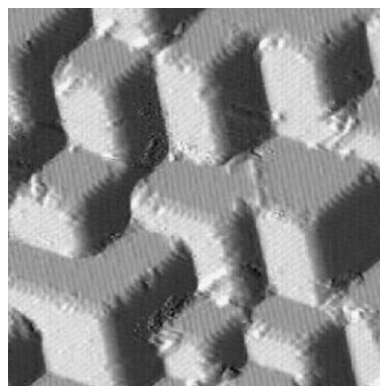


Fig. 3. STM image showing atomic-row structures on {211} facets. The Pd/W(111) surface is deposited with a Pd coverage of ~ 1.5 ML. Three-sided pyramids with {211} facets form upon annealing at 1075 K for several minutes. The dimensions of this image (x -slope filtered) are 25 nm \times 25 nm. The sample bias = +0.5 V.

Many experiments were carried out at different annealing temperatures. The facet sizes increase with temperature, as shown in Fig. 4 and Table 1.

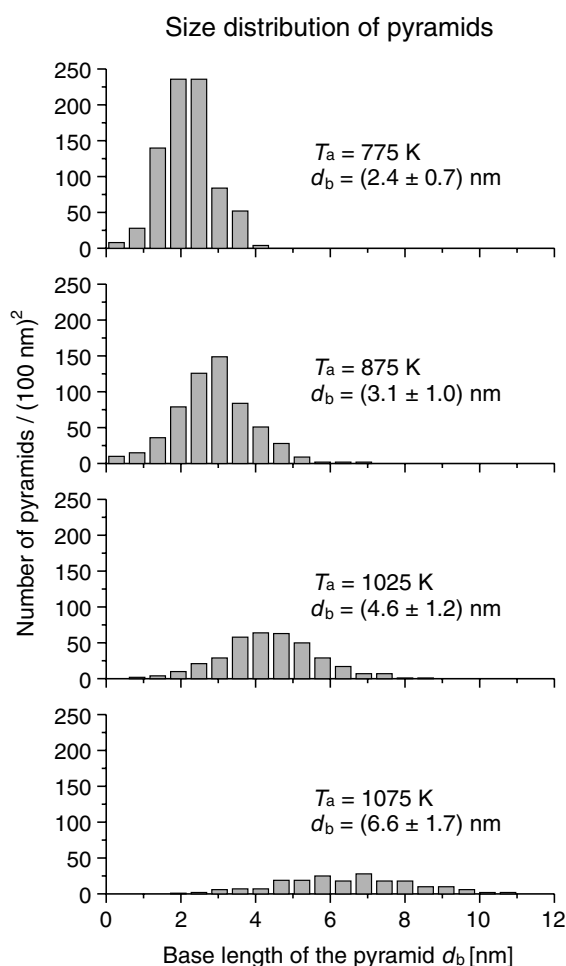


Fig. 4. Pd/W(111): the temperature dependence of the pyramid size distribution.

Table 1
Pd/W: The facet sizes increase with annealing temperature

Annealing temperature T_a [K]	Average size of pyramids d_b [nm]	Standard deviation $\sigma(d_b)$ [nm]	Surface rms roughness $rms(z)$ [nm]	$d_b/rms(z)$
775	2.4	0.7	0.078 ^a	31 ^a
875	3.1	1.0	0.179	17
1025	4.6	1.2	0.192	24
1075 (Exp. #1)	6.6	1.7	0.249	26
1075 (Exp. #2)	6.8	1.9	0.324	21
1075 (Exp. #3)	6.3	1.9	0.336	19

^a Uncertain value due to underlying stepped surface.

3.2. Curved surface: Microscopic data (FIM)

A detailed study of Pd/W faceting on a curved surface is described elsewhere [20]. Below we report only the facts relevant for comparison with STM data of Section 3.1.

In studying palladium-induced faceting of tungsten it is very important to make sure that there is no residual oxygen on the surface of the sample, otherwise oxygen-induced faceting will dominate over palladium effects. The crystal was carefully cleaned; blank experiments were carried out to rule out the possibility of faceting induced by residual oxygen.

Palladium deposition and annealing for 2 min at 1000–1200 K resulted in steplike {211} faceting in the vicinity of the (111) pole. The resulting topography in this region was found to be independent of the amount of deposited palladium, provided that a certain coverage was exceeded [20]. The topography was consistent with the scheme shown in Fig. 1(d), only the facet edges were slightly truncated, just as on a flat crystal (compare Fig. 3).

An example of Pd/W faceting is shown in Fig. 5. In this experiment, immediately after sample cleaning, 10 physical monolayers of palladium were deposited on the tungsten crystal (duration: 3.5 min). This was immediately followed by annealing for 2 min at 1100 K. After the crystal cooled down to liquid nitrogen temperature, surface topography was observed using FIM. Note the double $\langle 311 \rangle$ rows of atoms, signifying truncated $\langle 311 \rangle$ edges. In FIM it is not possible to measure accurately the width of a truncated edge due to giant local image distortion (local magnifi-

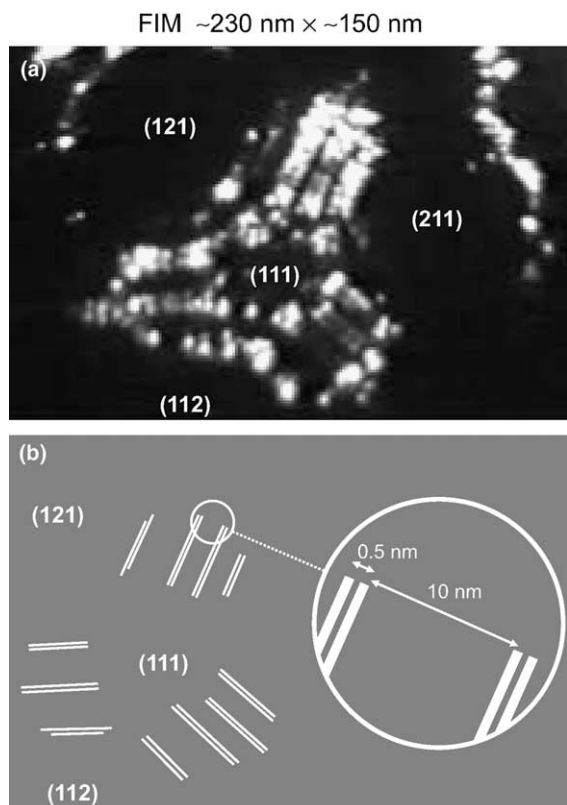


Fig. 5. Pd/W: (a) FIM image of a faceted surface after annealing at 1100 K ($\sim 80 \text{ K}$, He + Ne, 30 kV). Due to local magnification effects, the truncated $\langle 311 \rangle$ edges appear wide. (b) Approximate actual position of the edges on the crystal surface, after correction for ion trajectory deflections at surface edges.

cation) [20]. On the basis of STM data (Fig. 3), the width of the truncated $\langle 311 \rangle$ edge (Fig. 5) is about 0.5 nm, consistent with the interpretation that a single $\{211\}$ row of palladium atoms is missing at the edge.

The number of facets was smaller for experiments with higher annealing temperature T_a . The average number of $\langle 311 \rangle$ edges was $n_e = 6$ after annealing at 1000 K, $n_e = 5$ after annealing at 1100 K, and $n_e = 3.5$ after annealing at 1200 K. In Ref. [20] an approximate way of estimating the facet sizes was proposed, based on geometric considerations. Now we will take a more direct approach. As the average radius of curvature is known, it is possible to estimate the average magnification in FIM [38,39]. To estimate the distance

between the edges d_e and the length of the edges ℓ_e , we assume that the magnification of these lengths is equal to the average image magnification between the (112) and (121) crystal poles. Measurements yield $d_e = 9.3 \text{ nm}$, $\ell_e = 19 \text{ nm}$ after annealing at $T_a = 1000 \text{ K}$, $d_e = 9.6 \text{ nm}$, $\ell_e = 32 \text{ nm}$ after annealing at $T_a = 1100 \text{ K}$, and $d_e = 10.2 \text{ nm}$, $\ell_e = 26 \text{ nm}$ after annealing at $T_a = 1200 \text{ K}$.

4. Oxygen on tungsten

Oxygen has been long known to induce faceting of both curved [22,40–43] and planar [1–3,5,33] tungsten surfaces. Taylor reported $\{211\}$ facets forming on W(111) (exposure 0.3–1000 L, annealing at 800–1800 K) [1]. Tracy and Blakely observed faceting of W(100), W(112) and W(111) [2]. They also reported that W(110) is stable. For W(111), they found well developed $\{211\}$ facets for low oxygen exposure (0.5 L (Langmuir), where $1 \text{ L} = 1 \times 10^{-6} \text{ Torr s} = 1.33 \times 10^{-4} \text{ Pa s}$, 1020 K). For high exposures on W(111), they reported $\{110\}$ facets on $\{211\}$ facets; a similar structure has also been reported by Nien (60 L, 1380 K) [44]. Madey et al. observed well developed $\{211\}$ facets (0.6 L, 1200 K) [33]. Recently, Szczepkowicz and Bryl observed $\{211\}$ facets on a curved tungsten surface (1.3 L, 860–1800 K). In addition to steplike hill-and-valley faceting, they report global (convex) faceting (1.3 L, 1400–1600 K, $r = 0.2 \mu\text{m}$) [22]. Recent experiments [45] demonstrate that at temperature above 1000 K (111) vertices become rounded, in accordance with the theory of equilibrium crystal shapes [46]. The sharpness of the (111) vertices may be restored during cooling of the crystal, if the quenching rate is not very high.

4.1. Flat surface: Microscopic data (STM)

After cleaning of the planar W(111) surface [29], the crystal was exposed to 0.5 L (Langmuir) of oxygen at $\sim 350 \text{ K}$. Then the oxygen atmosphere was removed and the crystal was annealed for 180 s at 1075 K (800 °C). After the crystal cooled to room temperature, LEED and AES analyses were carried out. LEED observations clearly indi-

cated $\{211\}$ faceting of the surface, as observed previously [1,5].

This was then followed by STM analysis. One of the recorded images is shown in Fig. 6. One can clearly see that there are many pyramidal structures on the surface, which are ascribed to the O-induced faceting. There are large variations of the pyramid sizes. Most pyramids are small ($d_b \sim 4$ nm), but one can also find pyramids as big as $d_b \sim 16$ nm. The average linear-base-size d_b is 5.2 nm, standard deviation $\sigma(d_b)$ is 2.2 nm, and surface roughness $\text{rms}(z)$ is 0.2 nm. Note that there are many small round nanodots with apparent size ~ 2 nm (Fig. 6). These may be tiny pyramids, not resolved by STM, or may be a consequence of insufficient O coverage. In addition, cross-section analysis of the large and small pyramids suggests that the larger ones are more likely to be “well developed”, i.e., the ratio of the height to the base width (h/d_b) is close to the theoretical ratio.

4.2. Curved surface: Microscopic data (FIM)

A more detailed study of O/W faceting on curved surfaces is reported elsewhere [22,45,47,48]. Here we describe one new experiment, relevant for comparison with STM data of Section 4.1.

After thermal cleaning of the surface, the tungsten crystal was exposed to 0.7 ± 0.3 L of oxygen

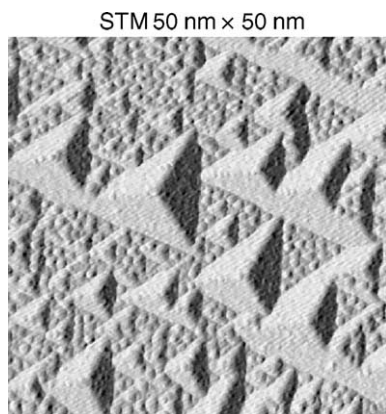


Fig. 6. Tungsten (111) surface after oxygen exposure (0.5 L) and annealing (1075 K, 180 s). Scanning tunneling microscopy at room temperature; α -slope-filtered view.

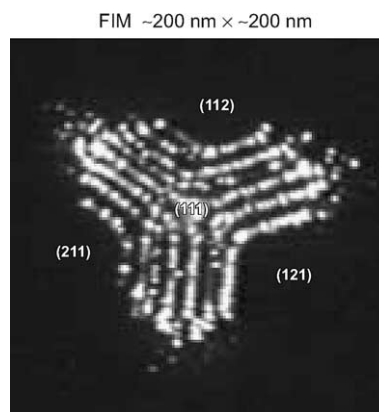


Fig. 7. Tungsten surface after oxygen exposure (0.7 ± 0.3 L) and annealing (1120 K, 80 s). Field ion microscopy at liquid nitrogen temperature (He + Ne, 32 kV). Edges of the facets are imaged as bright lines. The image covers the crystallographic orientations around the $W[111]$ direction within the angular radius of $20\text{--}30^\circ$.

at ~ 80 K (for such low coverages the oxygen sticking coefficient at 80 K is the same as at 350 K [49]). Then the oxygen atmosphere was removed and the crystal was annealed for 80 s at 1120 K. After the crystal cooled down to liquid nitrogen temperature (the estimated quenching rate is 400 K/s at 1000 K), surface topography was observed using FIM (Fig. 7).

The microscopic image reveals a heavily faceted topography. The global $\{211\}$ crystal facets are enlarged; they are separated by a steplike hill-and-valley region built of $\{211\}$ microfacets (compare Fig. 1(d)). The $\{211\}$ facets are interconnected by $[3\bar{1}\bar{1}]$, $[\bar{1}3\bar{1}]$ and $[\bar{1}\bar{1}3]$ edges. On the crystal surface shown in Fig. 7 there are six $[3\bar{1}\bar{1}]$ edges, seven $[\bar{1}\bar{1}3]$ edges, and eight $[\bar{1}3\bar{1}]$ edges; the average number of edges of one direction is $n_e = 7$. It is also possible to estimate the length of the edges and the separation between them, as described in Section 3.2. Measurement yields $d_e = 8.7$ nm and $\ell_e = 39$ nm.

5. Monte Carlo simulation for an adsorbate-covered bcc crystal

A simple solid-on-solid (SOS) model to describe faceting of bcc (111) crystal surface induced by an

adsorbate overlayer was proposed in Ref. [50]. The model assumes a pseudomorphic adsorbate overlayer with constant coverage equal to one physical monolayer (PML); it can be specialized to describe the case in which $\{211\}$ surfaces have low surface energy and the (111) face covered by one PML of adsorbate is not stable. This is consistent with the first principles calculations carried out for Pd/W [30]. In such a case, formation of three-sided $\{211\}$ pyramids was observed in Monte Carlo simulations of annealing bcc (111) crystal surfaces [50]. The sizes of pyramids depend on annealing temperature and annealing time. Another result obtained within this SOS model is the reversible phase transition at high temperature from faceted to the disordered phase as observed in a LEED experiment for Pd on Mo(111) [6]. Recently, it has been shown that this model can be applied to study faceting of curved bcc surfaces [25]. Results of Monte Carlo simulations are in qualitative agreement with experimental observations.

In order to compare adsorbate-induced faceting on a flat (111) surface with faceting on a spherical surface we performed Monte Carlo simulations for flat and curved crystals using the same annealing Monte Carlo time, number of surface atoms, temperature range and boundary conditions. Only the initial conditions were different. In the spherical case, the surface is formed by part of a sphere, around the (111) pole, determined by the radius $R = 290a$ (a is the bcc lattice constant) and the angular radius $\theta = 20^\circ$. To provide the same number of atoms and boundary conditions for a flat crystal, the bcc (111) surface has circular shape with a diameter $D = 2R \sin(\theta) = 198a$. Measurement of sizes of pyramids, distances between edges, etc. were performed at low temperature (we use here dimensionless temperature; for details see [50]). This means that after annealing at temperature T_a the system was quickly cooled down to reduce thermal disorder (a similar procedure was applied in STM and FIM experiments). All measured quantities were averaged over 1000 samples.

The initially flat surface after faceting consists of three-sided pyramids and three-sided pits of different sizes (see Fig. 8). Note the structure of atomic rows on the $\{211\}$ facets in Fig. 8(a), con-

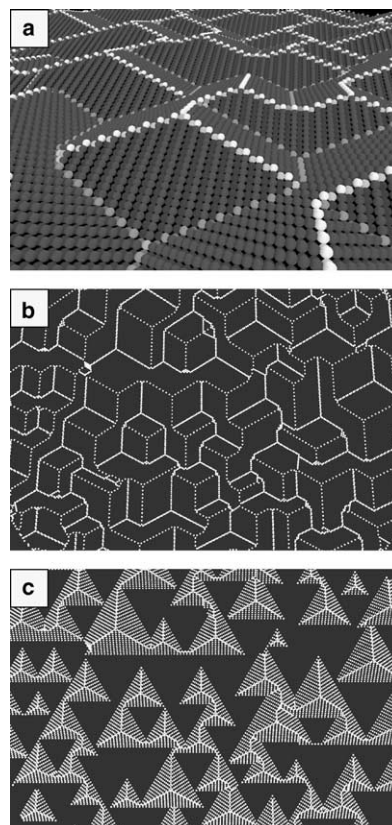


Fig. 8. Initially flat bcc (111) surface undergoes $\{211\}$ faceting. Images (a)–(c) show different graphical representations of the same faceted surface: (a) Angle view showing atomic details. All surface atoms are shown. (b) Top view. Only the edge atoms are shown. (c) Restricted top view. Only the atoms above the average surface height are shown.

sistent with the assumption of a pseudomorphic overlayer, and consistent with the STM images for Pd/W (Fig. 3). Distributions of pyramid sizes obtained in Monte Carlo simulations are presented in Fig. 9 and Table 2. The mean pyramid size d_b and its deviation $\sigma(d_b)$ increase with temperature similarly as in experimental measurements (compare Fig. 4). Note that the ratio $d_b/\text{rms}(z)$ is close to 24—the value calculated for the idealized case (Section 2).

In the case of a spherical crystal, we calculated the average distance d_e between two subsequent convex edges and the average number of parallel edges n_e as functions of annealing temperature

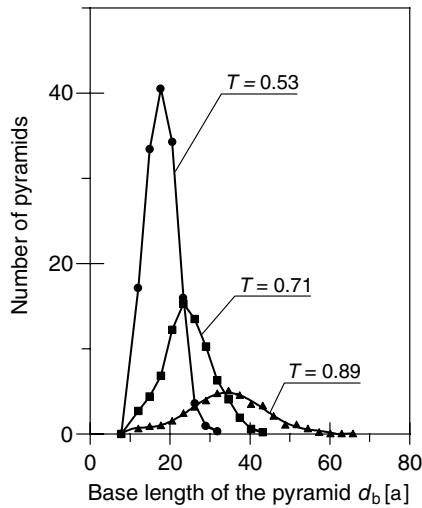


Fig. 9. Size distribution of pyramids calculated for $T = 0.53$, 0.71 and 0.89.

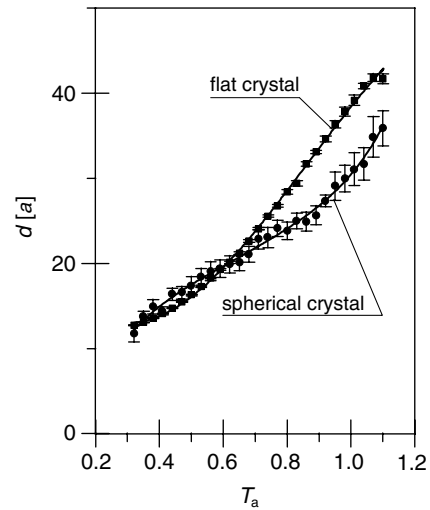


Fig. 10. Temperature dependence of pyramid base size d_b (squares), distance between parallel edges on curved surface d_c (circles).

T_a . Comparison of the mean distance between edges d_c with the mean pyramid base size d_b (presented in Fig. 10) shows that sizes of $\{211\}$ facets are nearly equal in flat and curved geometries. Differences, observed at higher temperatures, are below 20%. The average number of parallel edges decreases with temperature (see Fig. 11) as a result of formation of facets with larger sizes. We often observed transformation of neighboring $\{211\}$ steps into a single larger step. However, the shapes and areas of $\{211\}$ facets are different in the two cases of flat and spherical crystals (see Fig. 12), as discussed in Section 6.

It is worth noting that error bars for d_c are much greater than for d_b (Fig. 10), although the number of samples used to calculate the average values of $d_c(T_a)$ and $d_b(T_a)$ was the same. This is due to the fact that the formation of a larger facet is more difficult on a curved crystal, because the

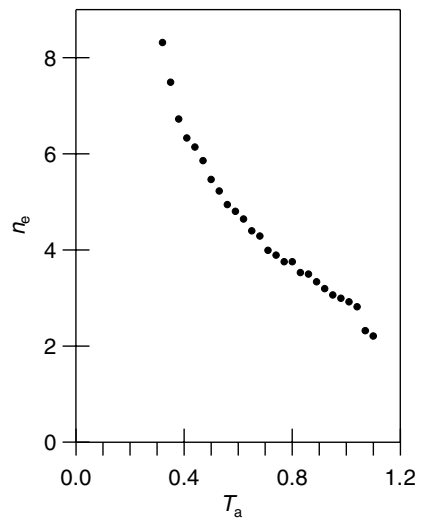


Fig. 11. Dependence of mean number of parallel edges on temperature.

Table 2
Simulation: the facet sizes increase with annealing temperature

Temperature (dimensionless) T	Average size of pyramids d_b (a)	Standard deviation $\sigma(d_b)$ (a)	Surface rms roughness $\text{rms}(z)$ (a)	$d_b/\text{rms}(z)$
0.53	17.5	3.80	0.77	22.7
0.71	24.2	6.14	1.08	22.4
0.89	33.9	9.52	1.50	22.6

The unit of length is the lattice constant a .

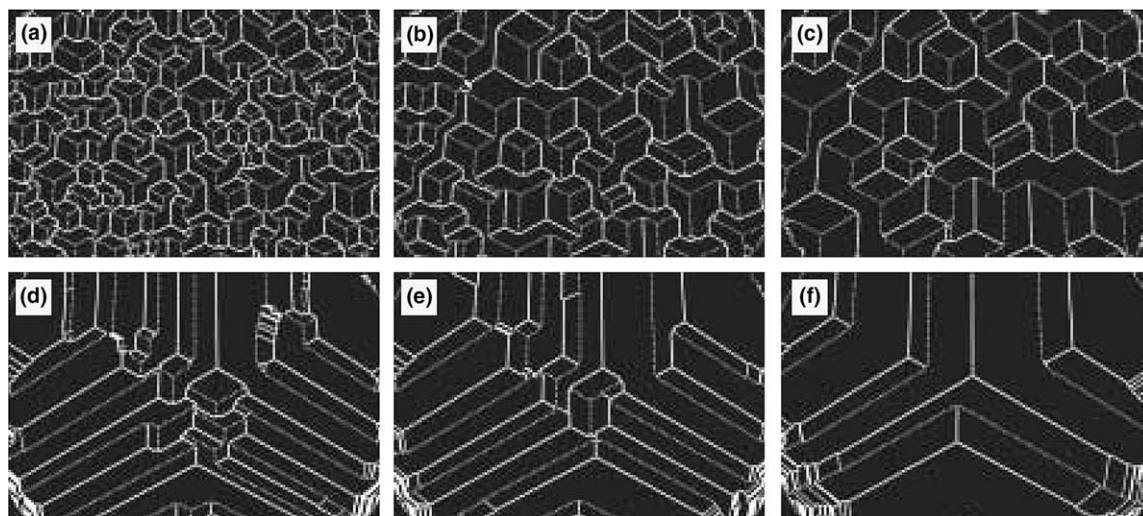


Fig. 12. The faceted topography after annealing at increasing temperatures. In (a)–(c) the surface was initially flat: (a) $T_a = 0.53$, (b) $T_a = 0.71$, (c) $T_a = 0.89$. In (d)–(f) the surface was initially spherical: (d) $T_a = 0.53$, (e) $T_a = 0.71$, (f) $T_a = 0.89$.

area of an elongated facet is much greater than the area of a pyramid on a planar surface at the same temperature (see e.g. Fig. 12(a),(d)). Therefore, the number of atoms needed to rebuild the surface of a curved crystal is much greater than in the case of a flat crystal, for equivalent projected areas. This is reflected in a steplike character of the $d_c(T_a)$ curve calculated for a single sample [25]. On the other hand, the average size of a pyramid for a single sample is a rather smooth function of T_a .

In both cases, flat and curved crystals, initially prepared surfaces covered by an adsorbate have higher total surface energies than the $\{211\}$ -faceted adsorbate-covered surface. This is the main reason that facets form after annealing to intermediate temperatures.

6. Discussion

6.1. Comparison of O/W and Pd/W faceting

Both oxygen and palladium induce the formation of W $\{211\}$ facets, and the resulting topography is similar in both cases. On a curved surface, the $\{211\}$ facets form a steplike hill-and-valley configuration, consistent with the scheme shown in Fig. 1(d). On planar W(111) crystals, three-

sided (211)–(121)–(112) pyramids are formed on the surface. For Pd/W, both concave and convex pyramids are observed (i.e. pyramids and pits), while for O/W under the present conditions only convex pyramids are seen—it is probable that in this case the surface is not fully faceted due to insufficient oxygen exposure (0.5 L). Recent FIM results for O/W [48] show that well developed $\{211\}$ facets are formed only in a narrow exposure range: 0.6–1.8 L. For Pd/W, the situation is different: the facet arrangement is independent of the coverage in a wide coverage range (1–10 PML), because the excess palladium agglomerates into clusters [20,28,30].

It is interesting to compare our results with a STM report of Pt/W(111) faceting [51]. The surface is fully faceted for Pt coverage ~ 1.1 PML, and the facet arrangement resembles that of Pd/W (Fig. 3). For Pt coverage ~ 0.8 PML, partial faceting is observed, with convex pyramids scattered on the otherwise planar surface. The number of pyramidal pits is much smaller than the number of convex pyramids. It appears that, for Pt/W, convex pyramids dominate at low adsorbate coverages, while the convex-concave symmetry is achieved at sufficient adsorbate coverage. It is probable that O/W exhibits a similar behavior, and at slightly higher oxygen exposure one can

expect a fully faceted topography with a convex-concave symmetry.

For Pd/W, the $d_b(\text{flat})/\text{rms}(z)$ ratio is 17–31; this is close to the “ideal” value 24 (Section 2), and to the Monte Carlo value 22.4–22.7. For O/W, although the topography is different (no pyramidal pits), a similar ratio is obtained: $d_b(\text{flat})/\text{rms}(z) = 26$.

There is a small scale difference between O/W and Pd/W pyramids: for Pd/W, the topmost chain of atoms at the $\langle 311 \rangle$ edges is missing, so that the facet edge is truncated (compare Figs. 3, 5 and 7). This effect was observed both on flat [28] and curved [20] surfaces. This feature, specific for Pd/W, cannot be reproduced by a simple SOS model based on pairwise potentials.

The desorption temperature of oxygen is much higher than that of palladium. It has been shown that thin oxygen adlayers are stable to above 1800 K ([52], polycrystalline W, coverage 3×10^{14} mol/cm²), and O/W faceting has been observed after annealing as high as 1800 K for 80 s [1,22]. For Pd/W, it has been established that one physical monolayer needed to stabilize $\{211\}$ facets remains on the surface only up to 1200 K [53,54], and this is the maximum temperature where palladium-induced faceting can be observed. Therefore, oxygen is capable of producing much larger facets (after annealing at high temperature). For curved surfaces of radius ~ 0.2 μm , the transition to global faceting (convex crystal, no valleys) is possible only for oxygen [20,22].

6.2. The shape of the facets

On an initially flat W(111) surface pyramid-like faceting is observed. In the idealized case shown in Fig. 1, where the pyramids form a regular array, all facets are of the same rhomboidal shape and the same size. In reality, where random atomic processes are involved during facet formation, there is no regular array of pyramids. As a consequence there is a certain spread of the pyramid sizes (Figs. 4 and 9), and a variety of facet shapes is observed (Figs. 3 and 8). With a good approximation, the facets can be described as 4, 6, 8, 10, ...-sided polygons; the edges of the facets run along the $\langle 311 \rangle$ directions. Every facet has

two kinds of edges. For example, as one goes around the perimeter of a (121) facet, one encounters an alternating sequence of $[3\bar{1}\bar{1}]$ and $[\bar{1}\bar{1}3]$ edges. For O/W, on a partially faceted surface shown in Fig. 6, triangular facets are observed. This may be due to insufficient oxygen exposure, as discussed in Section 6.1.

On a curved surface, the faceted topography changes with the crystallographic orientation. At the (111) crystal pole, the topography should be pyramid-like, as on a flat (111) crystal. This cannot be verified in FIM due to technical limitations, but the pyramidal facets clearly emerge in the model study—compare Fig. 12(a) with the center of Fig. 12(d). Note that the size of pyramids on both surfaces is comparable.

On each of the (211), (121), and (112) crystal poles, there is a huge ($\phi \sim 50$ – 100 nm) global facet of the corresponding orientation. These facets, only smaller, were already present on the initial clean surface. The shape of these facets could not be accurately determined; they can be roughly described as deformed circles.

The most striking changes of the curved surface occur halfway between the (112)–(121), (121)–(211) and (211)–(112) poles (Fig. 7). These are, respectively, the (233), (332) and (323) regions. The facet edges are very long there ($\ell_e \gg d_e$); the facets form elongated strips, arranged in a steplike configuration. Only the convex edges are visible in FIM; when there are n_e convex parallel edges, there are also $n_e - 1$ invisible concave edges of the same direction. The length ℓ_e of the edges in these regions is greatly influenced by the initial shape and size of the crystal. For example, for a cylindrical crystal axially oriented along (311) (one of the edge directions), arbitrarily long facet strips with (311) edges can be expected. Similar elongated facets have been detected in LEED studies of cylindrical crystals [16].

In our experiments, pyramid-like faceting is found on an initially flat crystal, while for a curved surface, steplike faceting dominates. This is not a general rule, however. For example, for other materials, ring-shaped facets have been reported on curved surfaces [17]; steplike faceting on a flat surface is also observed (e.g. [10]). For oxygen or palladium on a flat tungsten crystal, steplike

faceting is expected to occur for the orientation halfway between (121) and (211): for W(332). The topography will resemble a reflective diffraction grid; the grid constant d_c could be adjusted by proper thermal treatment of the crystal.

6.3. Comparison of the facet sizes for flat and curved surfaces

Let us begin with comparing the average facet area for flat and curved surfaces. We will apply equations of Section 2, first to the results of Section 3 (Pd/W), then to the results of Section 4 (O/W).

For palladium on flat tungsten (111), we obtain the area of a rhomboidal {211} facet formed after annealing at 1075 K: $A(\text{flat}) = \frac{\sqrt{6}}{8} d_b^2 = 0.306 \times (6.6 \text{ nm})^2 \approx 13 \text{ nm}^2$. For palladium on a curved tungsten surface, we obtain the area of a typical facet, having the shape of an elongated {211} strip, formed after annealing at 1100 K: $A(\text{curved}) = \frac{\sqrt{33}}{11} d_c \ell_c = 0.522 \times 9.6 \text{ nm} \times 32 \text{ nm} \approx 170 \text{ nm}^2$. So, for Pd/W, the ratio $A(\text{curved})/A(\text{flat})$ is ~ 13 .

For oxygen on flat tungsten (111), there are no pyramidal pits, so the average {211} facet is not rhomboidal, but triangular. The area of such a facet is half of a rhomboidal facet, and is equal to $A(\text{flat}) = \frac{1}{2} \frac{\sqrt{6}}{8} d_b^2 = 0.5 \times 0.306 \times (5.2 \text{ nm})^2 \approx 4 \text{ nm}^2$. For oxygen on a curved tungsten surface, we obtain the area of a typical facet, having the shape of an elongated {211} strip: $A(\text{curved}) = \frac{\sqrt{33}}{11} d_c \ell_c = 0.522 \times 8.7 \text{ nm} \times 39 \text{ nm} \approx 180 \text{ nm}^2$. So, for O/W, the ratio $A(\text{curved})/A(\text{flat})$ is ~ 45 .

Note that both for Pd/W and O/W $A(\text{curved})$ is much greater than $A(\text{flat})$; however, $A(\text{curved})$ depends on the average radius of curvature, because ℓ_c is influenced by the initial geometry, as discussed in Section 6.2. A similar result ($A(\text{curved}) \gg A(\text{flat})$) is obtained within the Monte Carlo model, as can be easily seen in Fig. 12.

Let us now compare the distance d_c between the adjacent facet edges for flat and curved surface. We will assume that $d_c(\text{flat}) = d_b(\text{flat})$, as in the idealized case shown in Fig. 2(c). The ratio $d_c(\text{curved})/d_c(\text{flat}) = d_c(\text{curved})/d_b(\text{flat})$ can be experimentally determined both for Pd/W and O/W, and is close to 1.7 in each case. The theoretical value of this ratio is in the range 0.8–1.1

(Fig. 10). The discrepancy between the experimental and theoretical value may be due to the simplified physics of the model, but it may also be caused by a systematic experimental error. Although the length scale calibration of STM is quite reliable, the measurement of distances in FIM is based on a simplifying assumption that the microscope magnification of d_c is equal to the average magnification between the (112) and (121) crystal poles. This is not strictly valid; one can expect local magnification, so our FIM value of $d_c(\text{curved})$ may be overestimated. Difficult numerical calculations of the ion trajectories in FIM would be necessary to solve this problem.

6.4. Dependence of the facet sizes on annealing temperature

It has been established previously that the facet sizes increase with annealing temperature T_a . This is equally true for flat (e.g. [55]) and curved ([14]) surfaces. Our data on Pd/W and the Monte Carlo results support this observation: the facet areas $A(\text{flat})$, $A(\text{curved})$, and the linear dimensions $d_b(\text{flat})$ and $d_c(\text{curved})$ increase with T_a ; the tendency is not clear with $\ell_c(\text{curved})$ – this edge length is probably more influenced by initial geometry than by the temperature of annealing, as discussed in Section 6.2. For O/W, FIM data [22] show that up to $\sim 1500 \text{ K}$ $d_c(\text{curved})$ increases with T_a ; at higher temperatures the behavior is more complicated, due to the fact that the facets are actually formed during quenching [25].

As facets increase in size, the total length of edges and the total number of vertices decrease (Fig. 12). For an initially flat crystal, the total length of the convex edges is equal to the total length of concave edges; also, the total number of convex vertices is equal to the total number of concave vertices. For an initially spherical crystal, there are more convex features (edges, vertices) than concave ones.

7. Conclusions

We have compared adsorbate-induced thermal faceting of flat and curved crystal surfaces, discuss-

ing four experimental examples: Pd/W(111), Pd/W(curved), O/W(111), O/W(curved), and presenting a simple solid on solid model which exhibits a similar faceting behavior. The most prominent features of observed surface restructuring are:

- {211} facets are observed on both flat and curved surfaces, but the shape of the facets depends on the initial surface shape.
- In both geometries the distance between the neighboring parallel $\langle 311 \rangle$ edges d_e is similar, although the area of a typical facet on a curved surface is an order of magnitude greater.
- In both geometries the extent of surface restructuring, as observed after cooling of the crystal, increases with annealing temperature T_a : the size of the facets, the width of the facet size distribution and surface rms roughness increase.

Acknowledgements

The work at Rutgers is supported in part by the US Department of Energy, Office of Basic Energy Sciences.

References

- [1] N.J. Taylor, Surf. Sci. 2 (1964) 544.
- [2] J.C. Tracy, J.M. Blakely, Surf. Sci. 13 (1968) 313.
- [3] H. Niehus, Surf. Sci. 87 (1979) 561.
- [4] E.D. Williams, N.C. Bartelt, Ultramicroscopy 31 (1989) 36.
- [5] K.-J. Song, R.A. Demmin, C. Dong, E. Garfunkel, T.E. Madey, Surf. Sci. Lett. 227 (1990) L79.
- [6] K.-J. Song, J.C. Lin, M.Y. Lai, Y.L. Wang, Surf. Sci. 327 (1995) 17.
- [7] T.E. Madey, J. Guan, C.-H. Nien, C.-Z. Dong, H.-S. Tao, R.A. Campbell, Surf. Rev. Lett. 3 (1996) 1315.
- [8] P. Knight, S. Driver, D. Woodruff, Surf. Sci. 376 (1997) 374.
- [9] T.E. Madey, C.-H. Nien, K. Pelhos, J.J. Kolodziej, I.M. Abdelrehim, H.-S. Tao, Surf. Sci. 438 (1999) 191.
- [10] N. Reinecke, E. Taglauer, Surf. Sci. 454–456 (2000) 94.
- [11] T.E. Madey, K. Pelhos, Q. Wu, R. Barnes, I. Ermanoski, W. Chen, J.J. Kolodziej, J.E. Rowe, Proceedings of the National Academy of Sciences of the United States of America 99 (2002) 6503.
- [12] Q. Chen, N.V. Richardson, Prog. Surf. Sci. 73 (2003) 59.
- [13] I. Ermanoski, K. Pelhos, W. Chen, J.S. Quinton, T.E. Madey, Surf. Sci. 549 (2004) 1.
- [14] A. Cetronio, J.P. Jones, Surf. Sci. 40 (1973) 227.
- [15] M. Drechsler, in: V.T. Binh (Ed.), Surface Mobilities on Solid Materials, Plenum Press, New York, 1983, p. 367.
- [16] S. Mróz, E. Bauer, Surf. Sci. 169 (1986) 394.
- [17] M. Drechsler, Surf. Sci. 266 (1992) 1.
- [18] K. Pelhos, T.E. Madey, R. Błaszczyszyn, Surf. Sci. 426 (1999) 61.
- [19] G. Antczak, T.E. Madey, M. Błaszczyszyn, R. Błaszczyszyn, Vacuum 63 (2001) 43.
- [20] A. Szczepkiewicz, A. Ciszewski, Surf. Sci. 515 (2002) 441.
- [21] G. Antczak, R. Błaszczyszyn, T.E. Madey, Prog. Surf. Sci. 74 (2003) 81.
- [22] A. Szczepkiewicz, R. Bryl, Surf. Sci. Lett. 559 (2004) L169.
- [23] A.K. Datye, D.J. Smith, Catal. Rev. Sci. Eng. 34 (1992) 129.
- [24] C. Henry, Surf. Sci. Rep. 31 (1998) 231.
- [25] D. Niewieczeral, C. Oleksy, 2005, Available from: <<http://arxiv.org/abs/cond-mat/0509023>>.
- [26] M. Sander, R. Imbihl, R. Schuster, J.V. Barth, G. Ertl, Surf. Sci. 271 (1992) 159.
- [27] R.E. Kirby, C.S. McKee, L.V. Renny, Surf. Sci. 97 (1980) 457.
- [28] C.-H. Nien, T.E. Madey, Surf. Sci. Lett. 380 (1997) L527.
- [29] Q. Wu, W. Chen, T.E. Madey, J. Phys. Chem. B 106 (2002) 6419.
- [30] C.-H. Nien, T.E. Madey, Y.W. Tai, T.C. Leung, J.G. Che, C.T. Chan, Phys. Rev. B 59 (1999) 10335.
- [31] C.-Z. Dong, J. Guan, R.A. Campbell, T.E. Madey, in: X. Xie, S.Y. Tong, M.A. van Hove (Eds.), The Structure of Surfaces IV, World Scientific, Singapore, 1994, p. 328.
- [32] K.-J. Song, C.-Z. Dong, T.E. Madey, Langmuir 7 (1991) 3019.
- [33] T.E. Madey, J. Guan, C.-Z. Dong, S. Shivaprasad, Surf. Sci. 287/288 (1993) 826.
- [34] C. Dong, L. Zhang, U. Diebold, T.E. Madey, Surf. Sci. 322 (1995) 221.
- [35] J.J. Kolodziej, T.E. Madey, J.W. Keister, J.E. Rowe, Phys. Rev. B 65 (2002) 075413.
- [36] E. Bauer, in: D.A. King, D.P. Woodruff (Eds.), Chemisorption Systems, The Chemical Physics of Solid Surfaces and Heterogeneous Catalysis, vol. 3B, Elsevier, Amsterdam—Oxford—New York, 1984, p. 1.
- [37] T.-Y. Fu, L.-C. Cheng, C.-H. Nien, T.T. Tsong, Phys. Rev. B 64 (2001) 113401.
- [38] E.W. Müller, T.T. Tsong, Field Ion Microscopy, Elsevier, 1969.
- [39] M.K. Miller, A. Cerezo, M.G. Hetherington, G.D.W. Smith, Atom Probe Field Ion Microscopy, Clarendon Press, Oxford, 1996.
- [40] J.A. Becker, Adv. Catal. 7 (1955) 135.
- [41] D.W. Bassett, Trans. Faraday Soc. 64 (1968) 489.
- [42] K.D. Rendulic, Surf. Sci. 21 (1970) 401.
- [43] R.A. Shigeishi, Can. J. Chem. 51 (1973) 997.
- [44] C.-H. Nien, Ph.D. Thesis, Rutgers—The State University of New Jersey, 1999.
- [45] A. Szczepkiewicz, R. Bryl, Phys. Rev. B 71 (2005) 113416.

- [46] M. Wortis, in: R. Vanselow, R. Howe (Eds.), *Chemistry and Physics of Solid Surfaces VII*, Springer, Berlin, 1988, p. 367.
- [47] R. Bryl, A. Szczepkowicz, *Appl. Surf. Sci.* 241 (2005) 431.
- [48] R. Bryl, A. Szczepkowicz, *Appl. Surf. Sci.*, submitted for publication.
- [49] A.M. Horgan, D.A. King, *Surf. Sci.* 23 (1970) 259.
- [50] C. Oleksy, *Surf. Sci.* 549 (2004) 246.
- [51] K. Pelhos, T.E. Madey, J.B. Hannon, G.L. Kellogg, *Surf. Rev. Lett.* 6 (1999) 767.
- [52] D.A. King, T.E. Madey, J.T. Yates, *J. Chem. Phys.* 55 (1971) 3236.
- [53] J. Kołaczekiewicz, E. Bauer, *Surf. Sci.* 420 (1999) 157.
- [54] K. Pelhos, I.M. Abdelrehim, C.-H. Nien, T.E. Madey, *J. Phys. Chem. B* 105 (2001) 3708.
- [55] C.Z. Dong, S. Shivaprasad, K.-J. Song, T.E. Madey, *J. Chem. Phys.* 99 (1993) 9172.